1
# Introduction

Neutron stars (NSs) are the stellar remnants or, end products of massive stars with masses in the range 8 to 20 $M_\odot$. They begin their lives in a dramatic manner known as supernova explosion. The remnants of these cataclysmic explosions (Type-II supernovae) possess mass between 1 to $\geqslant 2$ $M_\odot$ with radius in order of 10 km. Thus resulting in average matter densities of the order of $10^{14} - 10^{15}$ g/cm^3. *i.e.* higher than that found in atomic nuclei [Glendenning, 1996]. Stars with masses $\geqslant 20$ $M_\odot$ end being the densest objects in the universe, black holes (BHs). NSs also holds the record of strongest magnetic fields of $\sim 10^{15}$ Gauss. Moreover, the immense inward gravitational pull exerted by the remnant's mass is counter balanced by neutron degeneracy pressure due to the absence of any radiation pressure acting outward. Being highly compact in nature, NSs are able to spin-up to frequencies as large as (~ 700 Hz) [Hessels et al., 2006]. Thus, the relativistic effects become very crucial. Such extreme conditions can not be attained or reproduced in any of the terrestrial facilities now and will not be in the near future. These properties prove NSs to be ideal astrophysical laboratories for understanding several domains of physics. The high densities at the interior of NSs provide wide opportunities from probing ultra-dense matter behavior to exploring the gravitational effects that come into picture in binary NS (BNS) mergers resulting in gravitational radiations. These compact objects provide an extreme testing/developing ground to validate theories and underlying assumptions.

The exotic matter Quantum Chromo-Dynamic (QCD) phase diagram (refer to fig.-1.1) is not completely understood till date. Issues regarding understanding and determining the matter properties under extreme conditions (strong magnetic, gravitational fields, high rotational frequencies, surface temperatures) as found in NS interior has been a real challenge among physicists since decades. In an extensive perspective, the study of NSs covers a wide domain from micro-physics to astrophysics and provides ingress to grasp better knowledge in the higher ends of phase diagram as shown in fig.-1.1.
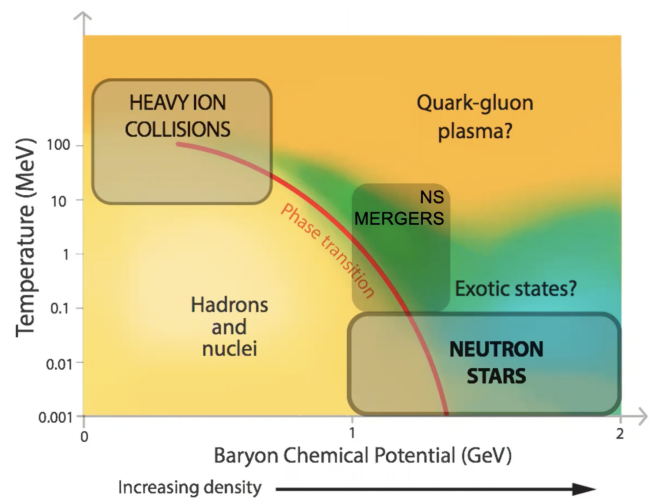

Figure 1.1: QCD phase diagram

1.1 Historical Background

After the discovery of neutrons by James Chadwick in the year 1932 [Chadwick, 1932], two astronomers Walter Baade and Fritz Zwicky hypothesized the concept of a high-density object consisting of closed packed neutrons, namely neutron star in 1934 by stating *"With all reserve we advance the view that supernovae represent the transition from ordinary stars into neutron stars, which in their final stages consist of extremely closely packed neutrons"* [Baade and Zwicky, 1934a,b]. It is suggested that Lev Landau had already anticipated the existence of a compact object independently in 1931 and published the next year [Landau, 1932]. Not long after hypothesizing the existence of NSs, Richard C. Tolman [Tolman, 1939], J. R. Oppenheimer and G. M. Volkoff [Oppenheimer and Volkoff, 1939] in the year 1939 derived the general relativistic equations of hydrostatic equilibrium for a spherically symmetric, non-rotating NS model. In a structure calculation, Tolman, Oppenheimer and Volkoff considered NSs to be consisted of degenerate non-interacting gas of neutrons which resulted in NS masses to be $\sim 0.7\ M_\odot$ much lesser than the Chandrashekhar's mass limit for white dwarfs (WDs) $\sim 1.44\ M_\odot$. This result indicated the vitality of considering nuclear forces or, particle interactions in describing NS matter. In the year 1958, John Wheeler and collaborators evaluated the dense matter equation of state (EoS) considering NS matter to be comprised of non-interacting nucleons and electron gas under β-equilibrium [Harrison et al., 1958]. A year later, A. G. W. Cameron studied the NS matter considering nucleon-nucleon interactions in Skyrme-type force framework and deduced an EoS which produces $\sim 2\ M_\odot$ stable NS configurations [Cameron, 1959]. Due to the high energy densities in NS interior, the concept of heavier degrees of freedom appearance can not be ruled out. The role of hyperons in dense matter EoS was first investigated by Cameron [1959] and Salpeter [1960] and followed by Ambartsumyan and Saakyan [1960] considering dense matter composition to be a concoction of baryons, mesons and lepton gases. The contribution of baryon-baryon forces on dense matter EoS considering hyperons as one fraction of matter composition in phenomenological interaction framework was perused by Tsuruta and Cameron [1966]. The role of yet another heavier non-strange degree of freedom, Δ-resonances in dense matter was first investigated by Glendenning [1985] and Glendenning and Moszkowski [1991]. The possibility of meson condensations interior to NSs were postulated by Migdal [1971], independently by Sawyer [1972] (π-condensation) and Nelson and Kaplan [1987]; Kaplan and Nelson [1988] ($\bar{K}$-condensation). Ivanenko and Kurdgelaidze [1965] suggested the existence of deconfined quarks in NS core after the proposal of quark model by Gell-Mann [1964]. This was followed by Bodmer [1971] and Witten [1984] hypothesizing the presence of strange quark matter in compact stars.

But it was not until 1967 that the existence of NSs were confirmed by the discovery of a radio pulsar (pulsating star) with a period of 1.33 seconds [Hewish et al., 1968] (Awarded Nobel Prize in 1974 to Anthony Hewish). The source of this radio radiation was speculated to be from an extra-terrestrial life form and whimsically designated as 'Little Green Man-1' or, LGM-1. Gold [1968] proposed the idea of pulsars being rotating NSs and that its respective rotational frequency should decrease with time as their electromagnetic radiation is backed up by rotational energy. It was proposed that pulsars are strongly magnetized NSs which emit focused electromagnetic radiation along the magnetic axis. Misalignment of the rotational axis with magnetic one gives rise to 'light-house effect' as observed from Earth. The idea of WDs being pulsars was eradicated based on the fact that such large centrifugal forces (due to high rotational periods) would disintegrate its entire structure. Riccardo Giacconi in the year 1971 discovered the X-ray pulsar, Cen X-3 [Giacconi et al., 1971] which was interpreted to be a rotating hot NS. Many more discoveries of these pulsars unveiled the extreme properties
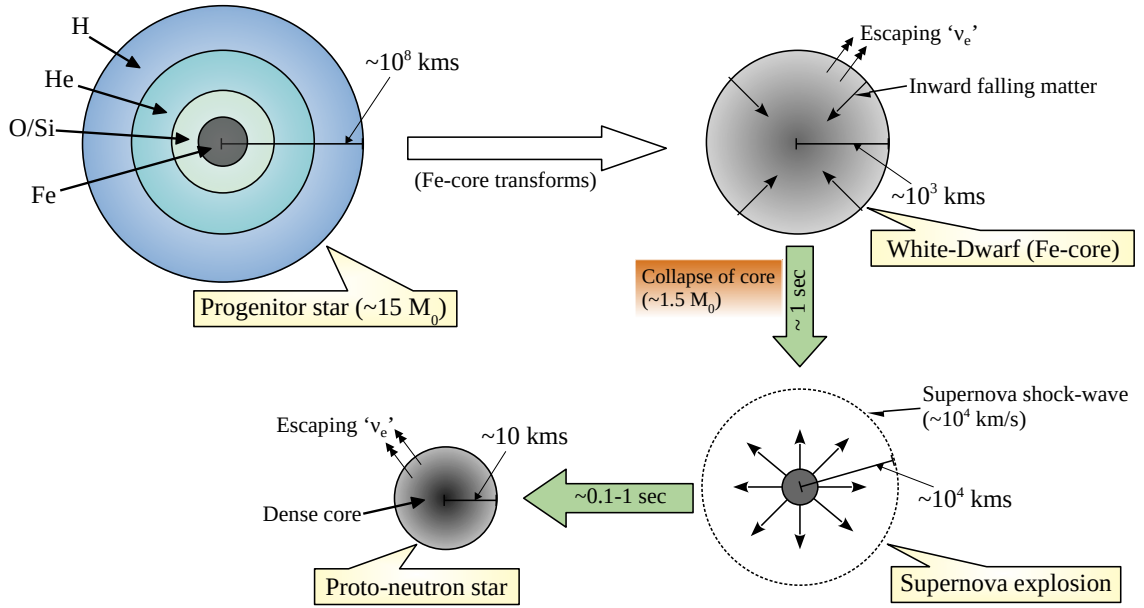
Figure 1.2: Schematic representation of NS formation from the onset of iron core-collapse. (Image not to scale)

associated with these compact objects identified as NSs. The discovery of a pulsar (PSR J1915+1606) in a binary system by R. A. Hulse and J. H. Taylor in the year 1974 [Hulse and Taylor, 1975] marked as an indirect test to prove the existence of gravitational waves (GWs) emission [Wagoner, 1975] (Hulse and Taylor were awarded the Nobel prize in 1993). The estimation of a slowdown rate in Crab pulsar's period [Lyne et al., 2015] and subsequent observation of Crab and Vela pulsars in remnants of supernova explosions [Haensel et al., 2007] confirmed the hypothesis put forward by Baade and Zwicky.

1.2 Formation of a neutron star

A star spends most of its life-time fusing hydrogen and thus maintaining thermal as well as mechanical equilibrium. Once the hydrogen is exhausted, the core mainly comprises of helium. At this stage, the helium core is surrounded by burning hydrogen shell. The star's dimension increases and it becomes a red giant. Next, the fusion of helium to higher atomic number elements depends on the progenitor star's mass. If the progenitor's mass is greater than 8 $M_\odot$, helium fuses to carbon and subsequent higher elements obtaining an onion-like structure until the entire core is made up of only iron with other lighter elements in the outer shells (refer to Fig.-1.2). Being the most tightly bound element in the Universe, the fusion process halts with the appearance of iron. At this point, due to the absence of any outward radiation pressure and gravity still acting inwards, matter in the outer shells starts falling into the core. This will continue until the core's mass reaches Chandrashekhar's mass limit (electrons become degenerate and ultra-relativistic) after which the electrons can not hold up against the gravitational pull. The core's temperature at this moment reaches $\sim 10^{10}$ K thus

enabling photo-dissociation of iron nuclei. This leads to emission of neutrinos cooling the core and increasing its density.

Neutrons are very unstable in free space and can decay into proton and electrons (β-decay). This is due to the fact that combined masses of a proton and an electron is around 1 MeV lower than the mass of neutron, so it is viable to decay. But at high density regimes interior to NSs, as $m_p + m_e + E_F > m_n$, from an energy argument point of view it is possible to combine a proton and an electron to form a neutron. Hence, we achieve neutron-rich nuclei at such high matter densities. Then at densities around $\sim 4 \times 10^{11}$ g-cm^{-3}, free neutrons drip out of the neutron-rich nuclei forming a sea of free neutrons. This point is the neutron drip point and beyond these densities, matter transforms into a smooth distribution of neutrons with some percentage of protons and electrons. As soon as the matter density ranges around $10^{11} - 10^{12}$ g-cm^{-3}, neutrinos can not escape the core. The core collapse continues until density approaches $\sim 10^{14}$ g-cm^{-3} at which point the neutron degeneracy pressure avoids the core from further collapsing. The in-falling matter bounces releasing a outward shock-wave deranging the progenitor's outer envelope in form of supernova explosion. The shock-wave heats up the envelope emitting intense electromagnetic radiation and ejecting matter into space. The remnants of these calamitous events will possess radii of $\sim 10 - 20$ km, masses of the order of $\sim 1 - 2 \ M_\odot$ and matter densities around $\sim 10^{14} - 10^{15}$ g-cm^{-3} [Glendenning, 1996; Haensel et al., 2007].

In brief, the following stellar stages are followed by massive stars resulting in NSs [Woosley and Janka, 2005]: Stellar nebula $\rightarrow$ Main sequence $\rightarrow$ Blue super-giant $\rightarrow$ Red giant $\rightarrow$ Type-II supernova $\rightarrow$ Neutron star.

1.3 Interior composition of neutron stars

Interior to NSs, the huge gravitational field developed by the large amount of matter is balanced solely by neutron degeneracy pressure as well as the particle interactions such as baryon-baryon, baryon-meson etc. Hence, it is obvious that matter interior to NS are mainly composed of neutrons. However, due to hydrostatic equilibrium the matter density varies – it increases gradually from surface to centre of the star. Consequently, depending on the density the composition and structure of matter we can divide the interior of NS in different regions [Glendenning, 1996], namely atmosphere and envelope, outer crust, inner crust, outer core and inner core (refer to fig.-1.3).

The atmosphere is merely a thin plasma layer of the order of millimeters to centimeters in thickness located just above the surface. This layer determines the electromagnetic radiation spectrum and related electromagnetic emission properties. Studying the NS atmosphere provides valuable information regarding thermal evolution of NSs, surface gravity, strength and geometry of the magnetic fields. It has been reported that the NS atmosphere may comprise lighter elements as heavier elements are viable to be dismantled via nuclear spallation processes [Bildsten et al., 1992; Servillat et al., 2012]. The density on the surface or envelope region is below the neutronization density of 10^7 g-cm^{-3} [Haensel et al., 2007] and so, matter in ionized ^{56}Fe nuclei form are crystallized in a Coulombic lattice with degenerate electrons.

The NS crust is composed of mostly nuclei and neutrons (less exotic) but is very crucial in understanding NS physics. Its thickness is around ~ 1 km and weighs few percent of the
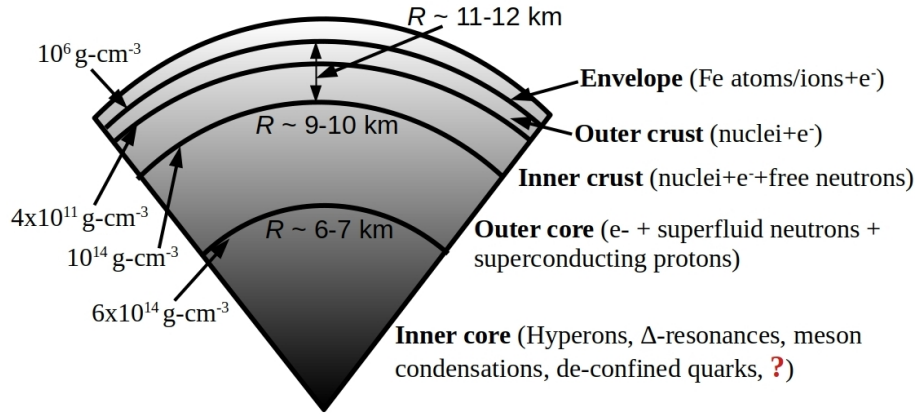
Figure 1.3: Schematic representation of NS internal structure and composition as a function of radial distance. (Image not to scale)

entire NS mass. The NS activities viz. glitches [Chamel and Haensel, 2008; Link et al., 1992] and thermal relaxations [Page et al., 2009; Page and Reddy, 2006] are reported to emanate from the NS surface. This region can be further categorized into outer and inner crust layers with matter densities around sub-saturation range. The outer crust is a layer of a few hundred meters in thickness with density range from 10^6 g-cm^{-3} to the neutron drip point of 4×10^{11} g-cm^{-3}. At these densities, ^{56}Fe nuclei are completely ionized with degenerate and ultra-relativistic electrons forming a solid crystal. Due to the initiation of neutronization process, the nuclei becomes neutron rich in nature with increasing density. The neutrons start to drip out of the nuclei at the inner boundary of this outer crust layer forming a neutron gas.

The inner crust region is signalized by the abundance of free neutrons. It is composed of a lattice of neutron-rich ions, free neutrons along with electrons. This layer lies in the density range of 4×10^{11} g-cm^{-3} to 10^{14} g-cm^{-3} or, ~ 0.5 times nuclear saturation density (core threshold density) [Haensel, 2001; Chamel et al., 2015]. The unbound neutrons can form Cooper pairs following $^1S_0$ angular momentum channel leading to superfluid state. It is suggested in studies [Ravenhall et al., 1983; Di Gallo et al., 2011] that the nuclei in this region attain deformed shapes as tubes or slabs (so-called pasta phases) to minimize the Coulomb energy.

Further interior to the NS, the nuclei disappear forming a sea of unbound neutrons and protons. This marks the initiation of core region. Its thickness is close to 10 km and most of the NS mass is concentrated in this layer. As in case of crust, this layer can also be divided into outer core and inner core parts. The outer core ranges from $0.5 - 2.0$ times saturation density and has a radial span around $9 - 10$ km. Matter in this layer comprises mainly of degenerate nucleons along with leptons such as electrons and muons ($npe\mu$-composition) to maintain β-equilibrium and charge neutrality in dense matter. The matter behavior at this region can be described within many-body nucleon interaction models. The neutrons in this layer retain superfluid nature via the $^3P_2$ channel [Sedrakian and Clark, 2019]. In addition to neutrons, the protons in this region can also form Cooper pairs following the $^1S_0$ channel leading to a charged superfluid (superconducting) state.

The inner core with matter densities greater than ~ 2 times saturation density and radial span of several kilometers is yet to be completely determined. The composition in this region is poorly known and mostly model dependent. Due to energy viability, several concepts

have been brought into consideration regarding appearance of exotic particles viz. strange baryons, meson condensations and even heavier non-strange baryons. Many authors have also put forward the phase transition hypothesis of hadronic matter to de-confined quark matter [Glendenning, 1996].

1.4 Neutron star structure

The NS structure can be obtained for spherically symmetric, non-rotating configuration by solving the Tolman-Oppenheimer-Volkoff (TOV) equations [Tolman, 1939; Oppenheimer and Volkoff, 1939]. These equations provide the stability between the inward gravitational pull and outward pressure sustaining NS configuration. Employing the Schwarzschild coordinates, the metric (line element) for static and spherically symmetric space-time is given by

$$ds^2 = g_{\mu\nu}dx^\mu dx^\nu = -e^{2\phi}dt^2 + \left(1 - \frac{2Gm}{r}\right)^{-1} dr^2 + r^2(d\theta^2 + sin^2\theta d\phi^2). \tag{1.1}$$

At the Newtonian limit, the gravitational mass enclosed within a radius r and the gravitational potential are given by $m(r)$ and $\phi(r)$ respectively. The approximation of considering NS matter to be a perfect fluid (*i.e* no viscosity or heat transfer) leads to manifestation of stress-energy tensor as

$$T^{\mu\nu} = (\varepsilon + P)u^\mu u^\nu + Pg^{\mu\nu}, \tag{1.2}$$

where $u^\mu \equiv dx^\mu/dt$ is the 4-velocity. This approximation is justified if the strain in the crust and magnetic pressure are negligible in comparison to matter pressure as well as the NS is considered to be non-rotating in nature.

Implementing the Einstein tensor which provides the bridge between energy-matter distribution and space-time curvature leads to the following TOV equations as

$$\frac{dP}{dr} = -[\varepsilon(r) + P(r)]\frac{d\phi}{dr} = -\frac{[\varepsilon(r) + P(r)][m(r) + 4\pi r^3 P(r)]}{r^2\left(1 - \frac{2m(r)}{r}\right)},$$

$$\frac{dm}{dr} = 4\pi r^2\varepsilon(r) \quad \text{or,} \quad m(r) = 4\pi\int_0^r \varepsilon(r')r'^2 dr', \tag{1.3}$$

where $\varepsilon(r)$, $P(r)$ denote the energy density and internal matter pressure respectively, within the spherical shell of radius r. The EoS (variation of pressure with energy density, $P(\varepsilon)$) has to be furnished due to fact that in order to solve for the three variables $m(r)$, $\varepsilon(r)$ and $P(r)$ only two equations are at hand.

In order to solve TOV equations as in eq.-(1.3), the boundary conditions for cold NSs usually are, $m(r = 0) = 0$, $P(r = 0) = P_c$ and $m(r = R) = M$, $P(r = R) = 0$ where P_c is the central matter pressure and M, R represent the total mass and radius of the star. *i.e.* the star's radius is determined by the latter conditions.

Observed NSs (pulsars, magnetars) are rotating stellar bodies so to describe the NS structure explicitly one needs to take rotation aspect into account. This demands for the Einstein field equations to be solved numerically. Bonazzola and Schneider [1974] and Butterworth

and Ipser [1976] in their pioneering works modelled rotating NS configurations considering incompressible polytropic EoSs. Due to the rotation, one can expect the spherical symmetry to be broken yet retaining axial symmetry. This symmetry breaking makes the structure equations very complicated which in turn affects the NS properties such as, the deformation of rotating NS, increase in mass due to rotation and the general relativistic effect of the dragging of local inertial frames. Rotation have significant impact on the properties of NS, *e.g.*, it can increase their masses, radii, decrease central density and notably change their shapes in comparison to non-rotating cases. The readers may refer to works Hartle [1967]; Hartle and Thorne [1968] to gather a comprehensive discussion and a detailed analysis on this particular aspect.

As mentioned earlier, being born from supernova explosions, NSs provide an idiosyncratic environment to study the exotic phases of matter at high densities which may range from a few to several times saturation density. The exact nature of inter-particle interaction at such high densities is not known precisely, though many authors have provided various phenomenological models based on density functional theories [Vautherin and Brink, 1972; Shen et al., 1998; Douchin and Haensel, 2001; Sun et al., 2008; Bao and Shen, 2014] and realistic nuclear potentials [Akmal et al., 1998; Li et al., 2006; Carlson et al., 2015; Hu et al., 2017; Logoteta, 2019] to explain and understand the nature of highly dense matter and internal structure of these compact stars. The internal temperature of proto-neutron stars formed just after the supernova explosions or, from binary NS mergers ($\sim$ few seconds) may reach up to few MeV, in which case we need to consider the contribution from neutrinos also as they can not escape (*i.e.* chemical potential of neutrinos is non-zero) to construct the finite temperature EoS. However, in this thesis we implement a relativistic mean-field theory model to describe the dense matter interior to NSs in zero temperature limit *i.e.* no neutrinos are trapped in the system. Further comprehensive discussions of this aspect will be addressed in chapter-2.

1.5 Equation of state constraints

The availability of experimental data and theoretical models provide us with a firm stage to determine the NS crustal properties and composition. But it is well known that matter densities interior to NSs goes from as low as 4 upto $\sim 8 - 9$ times nuclear saturation density. Such enormous density scenario can not be reproduced in any terrestrial laboratories and so to study dense matter behavior, the nuclear models have to be extrapolated to such high densities where neutron density greatly exceeds than that of proton. These extrapolations are required to be constrained to converge to a unique dense matter EoS. Around the saturation density regime, nuclear or heavy ion collision data provides an access to restrict bounds on EoS while for the case of high matter densities, one has to rely on astrophysical NS observables namely, masses, radii, rotational periods, surface temperatures, glitches and gravitational waves.

1.5.1 Heavy ion collision experiments

In recent years, the nuclear EoS has been reviewed and investigated extensively over the range of $0.25 - 4.5$ times nuclear saturation density in heavy ion collision and reaction experiments. These experiments probe matter in a restricted matter density range at finite temperature and provide the foundation for converging dense matter EoS and its properties. Symmetric nuclear matter has been constrained up to 4.5 times saturation density based on measurements of collective flow and kaon production in energetic nucleus-nucleus collisions

[Danielewicz et al., 2002; Le Fèvre et al., 2016; Russotto et al., 2016]. Similar measurements are also studied with kaon production at intermediate density range ($1.2 - 2.0$ times nuclear saturation) in [Fuchs, 2006; Lynch et al., 2009].

1.5.2 High isospin experiments

By observing the finite nuclei properties, one can infer to properties of nuclear matter. One of such important nuclear saturation properties is the symmetry energy which describes the isospin dependency of asymmetric nuclear EoS. It has to be noted that this parameter is not a directly measurable one and has to be estimated indirectly. One of the ways to make such an estimation is by measuring the neutron skin thickness ($\Delta R_{np} = R_n - R_p$). This parameter is largely dependent on proton asymmetry which can be exploited to comprehend matter behaviour at high density regimes [Sharma and Pal, 2009]. In contrast to proton radius R_p, the neutron radius R_n is very poorly known. Lead Radius EXperiment (PREX) based on parity violation in atomic systems estimated $\Delta R_{np} = 0.33^{+0.16}_{-0.18}$ fm [Abrahamyan et al., 2012]. Recently the updated PREX-II estimated the neutron skin thickness parameter to be 0.283 ± 0.071 fm [Adhikari et al., 2021]. It is noteworthy to mention that the structure of neutron rich as well as neutron deficient nuclei can be understood from the experiments based on rare isotopes [Wallace et al., 2007]. Refined results from future PREX and upcoming Calcium Radius EXperiment (CREX) CREX Collaboration [2021]; CRE [2021] may provide further insight in this regard.

## 1.5.3 Neutron star astrophysical observables

NS observations bestow an appreciable proportion of information for probing high density as well as high isospin matter behavior. With due course of time ~ 50 years, an enormous amount of data on different NS observables have been accumulated which encompasses masses, radii, rotational periods, surface temperatures, glitches and very recently, gravitational waves. Data from various observables lay the foundation for testing nuclear models for dense matter studies. These NS astrophysical observables are discussed in the next sections.

(a) Masses

NS masses can be indirectly measured from a binary system composed of a pulsar and a companion star. Based on the Keplerian parameters viz. orbital period, projection of the pulsar's semi-major axis on the line of sight, orbital eccentricity, longitude of periastron and time required for periastron passage, the binary orbit can be described precisely [Haensel et al., 2007]. Mass measurements are obtained in case of x-ray and optical binaries, binaries comprising of a pulsar and a companion star.

The Hulse-Taylor pulsar with measured mass 1.4408 ± 0.0003 $M_\odot$ [Hulse and Taylor, 1975] is one of the most precise mass measurements. Several massive pulsar measurements such as PSR J1614 $-$ 2230 ($M = 1.908 \pm 0.016$ $M_\odot$) [Demorest et al., 2010; Arzoumanian et al., 2018], PSR J0348 + 0432 (2.01 ± 0.04 $M_\odot$) [Antoniadis et al., 2013], millisecond pulsar J0740 + 6620 ($2.14^{+0.20}_{-0.18}$ $M_\odot$ with 95% credibility [Cromartie et al., 2020], $2.08^{+0.07}_{-0.07}$ $M_\odot$ with 68.3% credibility [Fonseca et al., 2021]) and PSR J1810 + 1744 (2.13 ± 0.04 $M_\odot$ with 68% credibility) [Romani et al., 2021] imply that the dense matter EoS must be stiff enough to produce the observed massive NS, $i.e.$ $M_{\max}(\text{EoS}) \geqslant M_{\max}^{\text{obs}}$. This puts a strong constraint
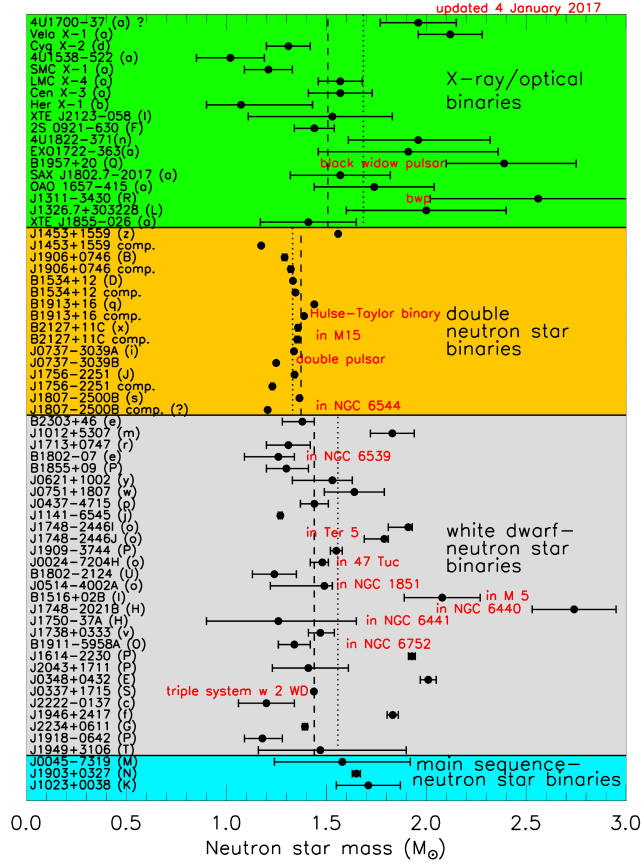
Figure 1.4: Representation of measured NS masses estimated from pulsar timing data. The vertical dashed and dotted lines represent the simple, weighted mass averages respectively. From Ref.-[Lattimer, 2019].

on the high matter density regime eradicating most of the softer EoSs. Fig.-1.4 provides the measured NS masses via pulsar timing in case of binary pulsars and X-ray binaries. The recent mass estimations of PSR J0740+6620 and PSR J1810+1744 are not included in this figure. The error-weighted average masses are seen to be around 1.4 $M_\odot$ for all measurement categories.

(b) Radii

From general relativity, a lower bound on the NS radii can be estimated to be greater than the Schwarzschild radius. *i.e.* $R > 2\, GM_{NS}/c^2$. While finite pressure constraint leads to a lower NS radius bound of $R > (9/4)\, GM_{NS}/c^2$ [Glendenning, 1996]. Causality constraint through the gravitational red-shift estimation and considering a causal EoS leads to a lower bound of $R > 2.9\, GM_{NS}/c^2$ [Haensel et al., 2007].

NS radii measurements can also be obtained by several procedures viz. gravitational red-shifts along with mass measurements, from the thermal emission spectrum of isolated NSs, type-I X-ray bursts or quiescent thermal emission from accreting NSs. Studies by Steiner et al. [2013]; Lattimer and Steiner [2014b] suggest NS radii of a canonical 1.4 $M_\odot$ to be around the range of $10.4 - 12.9$ km, while Guillot et al. [2013]; Guillot and Rutledge [2014] indicate the radii to be $\leqslant 10$ km. The latter studies imply the canonical NS to be very compact in nature
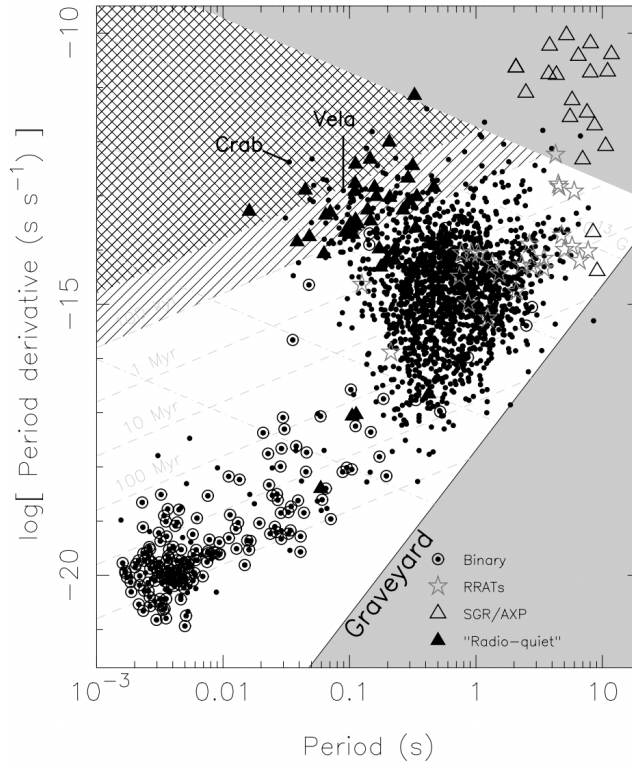
Figure 1.5: $P-\dot{P}$ diagram for the observed pulsar population. The characteristic age and surface magnetic fields are represented by dashed lines. The binary pulsars, Rotating RAdio Transients (RRATs) and magnetars are denoted by circle, star and up-triangles respectively. The 'pulsar graveyard' is represented by the lower grey region where the radio emissions from pulsars are expected to be switched off, while the upper grey region represents the NSs with surface magnetic fields larger than the quantum critical point of 4.4×10^{13} Gauss. The single dashed region denotes the 'Vela-like' pulsars with age $10-100$ kyr while the cross-dashed region depicts the 'Crab-like' pulsars with age below 10 kyr. From Ref.-[Lorimer and Kramer, 2004].

suggesting softer dense matter EoSs.

Precise information regarding mass and radius of NSs can also be extracted from recent Neutron star Interior Composition ExploreR (NICER) space mission. NICER provided vital information regarding the mass-radius estimations of PSR J0030 + 0451 to be in the range of $1.44^{+0.15}_{-0.14}\ M_\odot$, $13.02^{+1.24}_{-1.06}$ km [Miller et al., 2019] and $1.34^{+0.15}_{-0.16}\ M_\odot$, $12.71^{+1.14}_{-1.19}$ km (with 68.3% credibility) [Riley et al., 2019] respectively. Another very recent observation by NICER in the massive NS regime is for PSR J0740 + 6620 in the range of $2.072^{+0.067}_{-0.066}\ M_\odot$, $12.39^{+1.30}_{-0.98}$ km [Riley et al., 2021] and $2.08 \pm 0.07\ M_\odot$, $13.71^{+2.62}_{-1.50}$ km (with 68% credibility) [Miller et al., 2021] respectively.

(c) Rotational periods

High precision of pulsar timing data leads to the estimation stable rotational periods of radio pulsars. These estimations show the existence of different classes of pulsars namely, *magnetars* with $\sim 10s$ rotational periods, *normal* pulsars with $\sim 1s$, *millisecond* pulsars with 1000 order less than *normal* ones (refer to fig.-1.5). Based on the spin frequency or, rota-
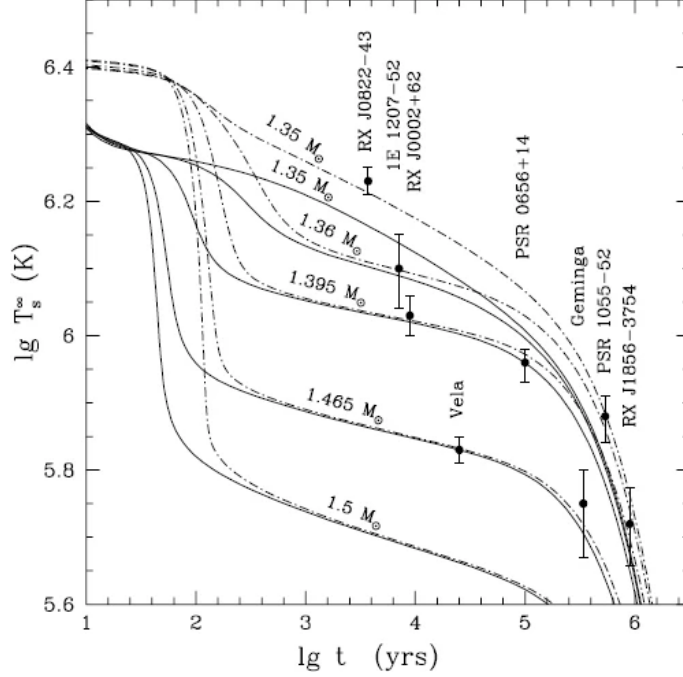
Figure 1.6: Effective NS surface temperatures, T_S^∞ (in units of Kelvin) as a function of the age of NSs (in units of years) for various NS mass configurations. The observational constraint of eight NSs on surface temperature is implemented in this figure. The solid curves represent the different cases considering neutron superfluidity in the crust and core, while the dot-dashed ones denote the cases assuming only proton superfluidity in the core. From Ref.-[Chamel and Haensel, 2008].

tional periods, stringent constraints on the radius of a stable NS configuration can be deduced. [Hessels et al., 2006] observed the fastest pulsar PSR J1748 − 2446ad until today with spin frequency ∼ 716 Hz.

An empirical relation was derived by [Lattimer and Prakash, 2004] to estimate the upper bound on non-rotating NS from observed rotational periods as,

$$R_{\mathrm{NR}} < 10.4 \left(\frac{1000 \text{ Hz}}{f} \right)^{2/3} \left(\frac{M_{\mathrm{NR}}}{M_\odot} \right)^{1/3} \text{km}, \tag{1.4}$$

where NR subscript represents the non-rotating parameter. Plugging in the observed value of spin frequency, the upper bound on NS radii is estimated to be $R_{\mathrm{NR}} < 13 \, (M_{\mathrm{NR}}/M_\odot)^{1/3}$ km.

(d) Surface temperatures

Measuring the NS surface temperatures could also provide vital information to estimate the exotic properties of matter in NS interior. This physical observable is detected from the thermal photons emitted from surface of X-ray binaries. The NS surface temperature is close to 10^{12} K at the proto-neutron star (birth) stage. But it is observed that within a short span of 1000 years, the surface temperature goes down to ∼ 10^6 K (refer to fig.-1.6). This rapid cooling is speculated to majorly occur due to neutrino emission processes in the core of the NS [Yakovlev and Pethick, 2004; Page et al., 2009]. From fig.-1.6, it can be seen that the heavier NSs cool faster in comparison to lighter ones. After a span of $10^4 - 10^5$ years, the dominant
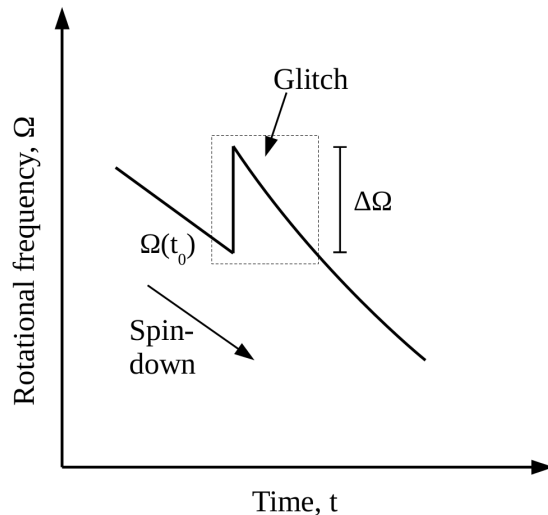
Figure 1.7: Schematic representation of *glitch* phenomena in pulsars. (Image not to scale)

cooling process in NSs remains to be via emission of diffused thermal photons from NS interiors.

(e) Glitches

Pulsars emit electromagnetic radiation from their magnetic poles at the expense of their rotational energy which in turn leads to decrease in rotational frequency or, spin-down of pulsars. It is observed that in the spin-down process of most relatively young radio pulsars, sudden rise in rotational frequencies or jumps appear followed by a slow relaxation persisting for an appreciable span of time (refer to fig.-1.7). These jumps in rotational frequencies are known as *glitches*. As they do not affect the pulse profile of the pulsars, we say that they have the potential to offer an intuition in understanding the internal dynamics of NSs thereby constraining the dense matter properties. The relative increase in rotational frequencies may vary from $\Delta\Omega/\Omega \sim 10^{-10}$ to as large as $\sim 10^{-6} - 10^{-5}$. Radhakrishnan and Manchester [1969] observed the first glitch from Vela pulsar ($\sim 10^{-5}$) and the Crab pulsar's relative glitch rise time was estimated to be $\sim 10^{-8} - 10^{-9}$ [Boynton et al., 1972]. For updates on *glitch* observations in pulsars, the reader may refer to refs.-[Espinoza et al., 2011; Yu et al., 2013; Basu et al., 2021].

The exact origin of *glitch* phenomena in pulsars is not completely understood yet. With the detection of *glitches* in Vela and Crab pulsars, starquake or, crust quake [Baym et al., 1969] was proposed to be the viable cause. But this model was unable to explain the large *glitches*. However, Anderson and Itoh [1975]; Alpar [1977] have provided with a propitious model based on the formation of neutron superfluid vortex lines in the inner crust region of NSs. This model considers the transfer of angular momentum of the unpinned vortices to the crust by the excess magnus force acting on them, thus increasing the overall rotational frequency of the NS. The unpinning of the vortex lines is followed by thermal creep against the pinning energy barriers. The giant *glitches* of Vela like pulsars are still not well modelled. In order to elucidate those, in addition to the contribution of angular momentum from the crust, the contribution from the core region should also be brought into the picture.
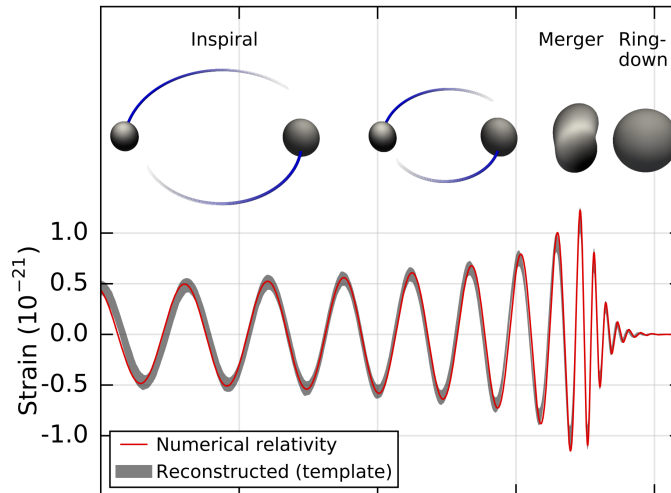
Figure 1.8: GW signal reconstruction and interpretation of GW150914 event as different stages, inspiral, merger and ringdown. From Ref.-[Abbott et al., 2016].

(f) Gravitational waves

When massive stellar objects move, due to their intense gravitational fields, they produce fluctuations or, 'ripples' in space-time. These ripples are known as *gravitational waves* (GWs) and they travel with the speed of light. The different stages involved in a GW merger event is shown in fig.-1.8. The observations of GWs from merger of compact objects (NS-NS or, NS-Black Hole (BH)) as well as from isolated asymmetric NSs may provide with intriguing information regarding dense matter behavior. GWs were first postulated by Albert Einstein in the year 1916 but no direct detections had been made until very recently.

The outstanding observation of GW signal from a binary coalescence of NSs on August 17th 2017 by the Advanced LIGO [LIGO Scientific Collaboration et al., 2015] - Virgo [Acernese et al., 2015] collaboration (GW170817) [Abbott et al., 2017c] lead the way to a new era of multi-messenger astronomy. The upper limit of tidal response observable ($\tilde{\Lambda}$) estimated from this event for low-spin prior systems is to be around 900 [Abbott et al., 2017c] while recent reanalysis put the bounds in the range of $70 - 720$ at 90% confidence interval and 90% highest posterior density interval [Abbott et al., 2019]. Based on the subsequent electromagnetic radiations [Abbott et al., 2017a,b; Coulter et al., 2017] from GW170817 event, the lower bound on $\tilde{\Lambda}$ is deduced to be 400 [Radice et al., 2018]. Furthermore, gamma-ray bursts and kilonova exemplified it to be a formation site for heavy elements [Kasliwal et al., 2022; Watson et al., 2019]. Another GW event involving binary NS merger was observed on 25th April, 2019 (GW190425) [Abbott et al., 2020a]. This event put an upper bound of 600 on $\tilde{\Lambda}$ in the case of low-spin prior configurations. The secondary component of GW190814 event (NS-BH) puts an upper limit on possible compact star maximum mass configuration with mass $2.59^{+0.08}_{-0.09}\ M_\odot$ [Abbott et al., 2020b]. Since this falls in the 'mass-gap' region, the nature of the secondary component is yet to be resolved. Very recently, two events namely GW200105 and GW200115 [Abbott et al., 2021] were observed by the LIGO-Virgo collaboration from NS-BH coalescences with mass of the NSs involved being $1.9^{+0.3}_{-0.2}\ M_\odot$ and $1.5^{+0.7}_{-0.3}\ M_\odot$ respectively.

Even before the detection of GWs from binary NS mergers (GW170817 [Abbott et al., 2017c], GW190425 [Abbott et al., 2020a]), it was appraised that binary NS systems may be

good and promising sources of GW emissions [Cutler et al., 1993]. Due to the fact that NSs tend to behave as extended bodies in presence of external gravitational field, the GW emission from binary NSs mergers differs to that of binary BH coalescences. The tidal deformations that each star induces on the other can account for the finite deviations of GWs from the binary BH case. The finite size effect is a direct consequence of the star's matter distribution, so it can be ascertained that GWs can in effect probe NS interior.

Tidal deformation parameter

If we consider a star in an external quadrupolar tidal field $\mathcal{E}_{ij}$, then a mass quadrupole moment Q_{ij} is developed by the star which to a linear order can be related as [Hinderer, 2008; Hinderer et al., 2010]

$$Q_{ij} = -\frac{2}{3}k_2 R^5 \mathcal{E}_{ij}, \tag{1.5}$$

where k_2 (corresponding to $l = 2$) denote the tidal Love number. The tidal effects can be quantified in terms of tidal deformability parameter (λ) defined as, $\lambda = Q_{ij}/\mathcal{E}_{ij}$. The tidal Love number is given by

$$
\begin{aligned}
k_2 =& \frac{8C^5}{5}(1-2C^2)[2+2C(y-1)-y] \cdot \{2C[6-3y+3C(5y-8)] \\
& + 4C^3[13-11y+C(3y-2)+2C^2(1+y)] + 3(1-2C^2) \cdot \\
& [2-y+2C(y-1)]\ln(1-2C)\}^{-1}
\end{aligned}
\tag{1.6}
$$

with $C = M/R$ being the compactness parameter, M and R being mass and radius of the star respectively. $y = y(R)$ is the function obtained after solving the differential equation [Binnington and Poisson, 2009; Damour and Nagar, 2010]

$$r\frac{dy(r)}{dr} + y(r)^2 + y(r)F(r) + r^2 Q(r) = 0, \tag{1.7}$$

where the functions are

$$
F(r) = \frac{r - 4\pi r^3[\varepsilon(r) - P(r)]}{r - 2M(r)}, \quad Q(r) = \frac{4\pi r[5\varepsilon(r) + 9P(r) + \frac{\varepsilon(r)+P(r)}{\partial P(r)/\partial\varepsilon(r)}]}{r - 2M(r)} \\
- 4\left[\frac{M(r) + 4\pi r^3 P(r)}{r^2(1-2M(r)/r)}\right].
\tag{1.8}
$$

Due to paramount dependence on the stellar radius, λ imposes stringent constraints on dense matter EoS. λ or, equivalently k_2 provides the ease of induced deformation estimate of bulk matter. This parameter is evaluated self-consistently alongside the TOV equations. Another dimensionless quantity Λ is much more expedient as it relates λ with C through the relation

$$\Lambda = \frac{\lambda}{M^5} = \frac{2}{3}\frac{k_2}{C^5}. \tag{1.9}$$

GW signal encodes information regarding deformation of both compact objects in the binary system as the weighted tidal deformability ($\tilde{\lambda}$) and is given by [Hinderer, 2008; Hinderer et al., 2010]

$$\tilde{\lambda} = \frac{1}{26}\left[\frac{M_1 + 12M_2}{M_1}\lambda_1 + \frac{M_2 + 12M_1}{M_2}\lambda_2\right], \tag{1.10}$$

where λ_1 and λ_2 are the tidal deformabilities corresponding to stars with masses M_1 and M_2 respectively. In order to relate to Λ, we incorporate the combined dimensionless tidal deformability ($\tilde{\Lambda}$) defined as

$$
\begin{aligned}
\tilde{\Lambda} &= 32 \frac{\tilde{\lambda}}{(M_1 + M_2)^5} \\
&= \frac{16}{13} \frac{(M_1 + 12M_2)M_1^4 \Lambda_1 + (M_2 + 12M_1)M_2^4 \Lambda_2}{(M_1 + M_2)^5}.
\end{aligned}
\tag{1.11}
$$

1.6 Objectives

This thesis work is concerned with the study of highly asymmetric nuclear matter within the framework of relativistic mean field (RMF) theory implementing non-linear scalar and density-dependent baryon-meson coupling schemes. The theoretical deductions acquired from these models are collated with the data from finite nuclei experiments and various astrophysical observations. Due to high neutron Fermi energy interior of NSs, the appearance of particles such as (anti)kaons, heavier strange (hyperons) as well as non-strange (Δ-resonances) baryons become feasible. We further extend the models incorporating these exotic degrees of freedom and study their impact on different NS observables. The subsequent chapters are briefly outlined as follows.

In chapter-2, we provide a brief summary of the RMF model implemented to evaluate the dense matter EoS in this thesis work. We also collect the basic ideas from RMF approach employed to evaluate the energy of the system. In this chapter, we further describe the non-linear and density-dependent coupling models providing a list of parameterizations (parameter sets) used in our calculations.

We devote chapter-3 to the study of meson (antikaon) condensation in NS matter in the context of the recent astrophysical observations. The consequences of non-linear scalar as well as density-dependent baryon-meson couplings with the possibility of (anti)kaon condensation are discussed in this chapter, while the (anti)kaon couplings to mesons are considered to be density-independent in nature. This is followed by a discussion on the obtained results.

The viability of hyperons and Δ-baryons in NS dense matter is presented in chapter-4. The formalism for these inclusion of heavier baryons in RMF framework is described followed by discussing the implications on astrophysical observables and nuclear properties. The baryon-meson couplings are constrained based on the recent astrophysical observations. The interplay between these heavier baryons and meson condensation is also reviewed in this chapter. In this case, the baryon-meson couplings are considered to be density-dependent in nature while that of (anti)kaon-meson are assumed to be density-independent.

GW detection from binary NS merger events has opened up a unique window to explore the NS matter. This has lead to constrain theoretical dense matter EoS models extensively as it has amplified the contemporary attention to examine the sensitivity of the EoS at large values of the density and of the isospin asymmetry. In chapter-5, we discuss the implications of GW observables on baryonic dense matter. We consider both the non-linear scalar and density-dependent coupling cases in presence of additional heavier particle spectrum and scrutinize the parametrizations which fulfil the astrophysical as well as nuclear physics experiment data.

Very recently an improved value of neutron skin thickness of ^{208}Pb was reported in Lead Radius EXperiment-2 (PREX-2) [Adhikari et al., 2021]. Reed et al. [2021] reported the corresponding symmetry energy and its slope to be $E_{\mathrm{sym}} = (38.1 \pm 4.7)$ MeV and $L = (106 \pm 37)$ MeV respectively at nuclear saturation density (n_0) with correlation coefficient as 0.978. Chapter-6 is dedicated to study the effects of updated PREX-2 data on NS matter EoS and related properties such as particle fraction profiles, NS observables followed by comparison with the astrophysical observations.

NSs are also reported to possess strong magnetic fields. A particular class of NSs, known as *magnetars* hold the strongest magnetic fields in the Universe. The effects of intense magnetic field on NS matter with exotic degrees of freedom is presented in chapter-7.

And finally the conclusions and possible extensions of of this thesis work are encompassed in chapter-8.